Validation of ASTM F2267 models in Alfonso™: Uniaxial subsidence of titanium spinal spacers

Non-Confidential Technical Whitepaper – 12 April 2023

Experiments and Analysis: Janice Oentaryo, PhD; Rezaul Tharim; Sloan Kulper, PhD; and Erica Ueda Boles, PhD
Visualizations: Abbas Alvi and Eka Tjong

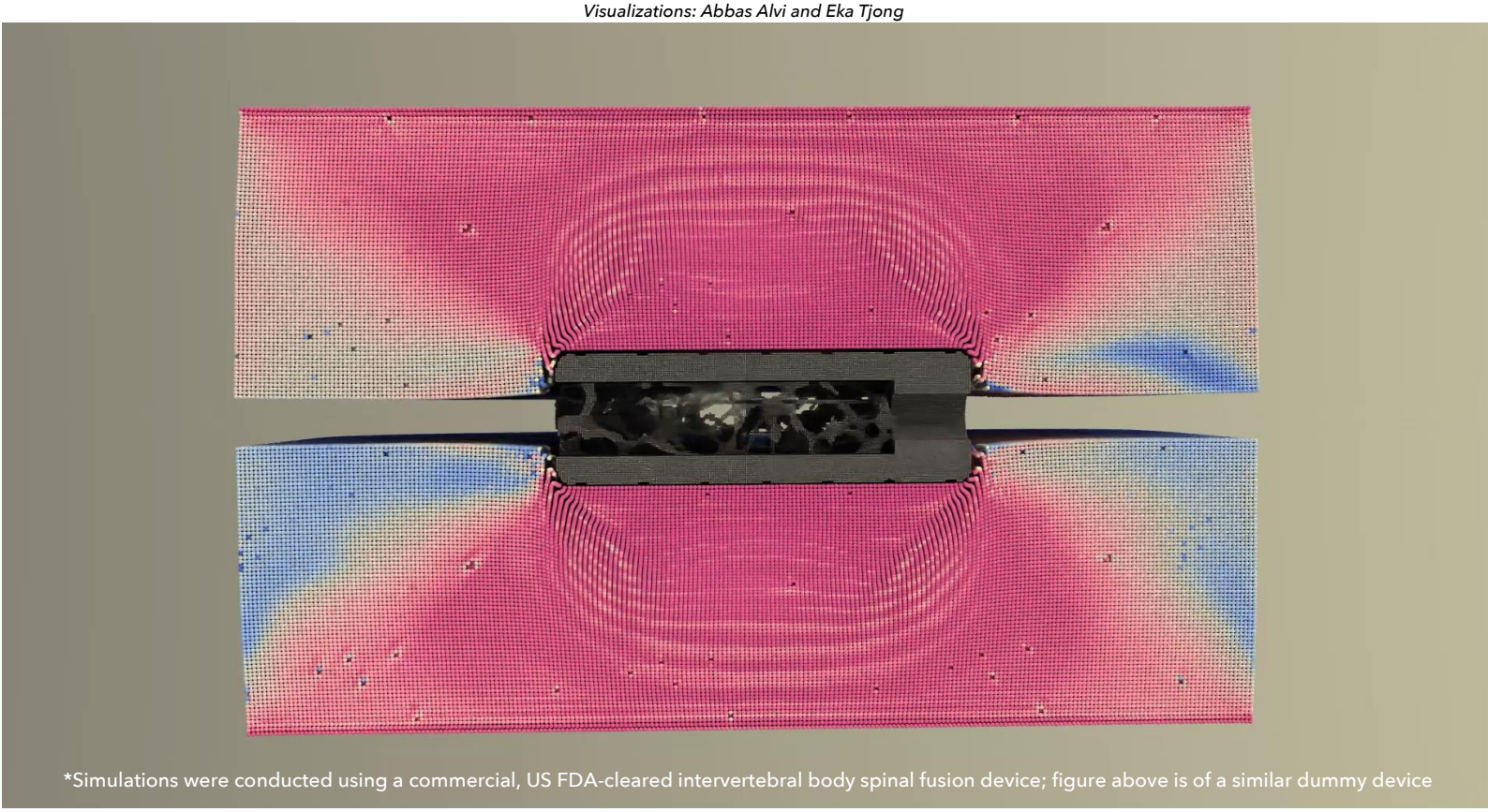

*Simulations were conducted using a commercial, US FDA-cleared intervertebral body spinal fusion device; figure above is of a similar dummy device

Abstract

Computational models of the static axial subsidence tests of several sizes of additively manufactured Ti-6Al-4V ELI (e.g., material per ASTM F3001-14-2021) lumbar intervertebral body fusion devices were tested using the *Alfonso*™ particle-based simulation system and validated via comparison to experimental data. Commercially available US FDA-cleared 3D-printed titanium devices of three different sizes (H13, H11, and H7 mm; n=5 specimens for each group) were tested by an independent laboratory according to the ASTM F2267-22 standard. Devices were axially compressed at a loading rate of 0.1 mm/s until a certain displacement (10 mm, 8 mm, and 5 mm for H13, H11, and H7 mm spacer, respectively) was reached or unnatural tilting of the implant was observed. Prior to testing, micro-CT scans were collected for each specimen at a resolution of 182 µm/pixel and then converted to particle models in *Alfonso*™ for simulated ASTM F2267-22 static axial compression, using a material model based on the typical properties of Ti-6Al-4V ELI. The average stiffness value of the system (K_s) for the H13 mm device was 533 and 420 N/mm with average yield load of 1,690 and 1,821 N at average yield displacement of 5.1 and 6.5 mm in the physical and simulated test, respectively. The average K_s value for the H11 mm device was 916 and 443 N/mm with average yield load of 1,408 and 1,679 N at average yield displacement of 3.4 and 5.7 mm in the physical and simulated test, respectively. The average K_s value for the H7 mm device was 586 and 457 N/mm in the physical and simulated tests, respectively. The average CCC (concordance correlation coefficient) between the force-displacement curves for the simulation and experiment was >0.95, suggesting excellent concordance. *Alfonso*™ can accurately predict the subsidence of various porous 3D-printed titanium intervertebral body fusion devices based on implant geometry and standard material properties.

Background and objectives

ASTM F2267-22 is a standard test method used to evaluate the performance of non-biologic intervertebral body fusion devices (e.g., under FDA product code MAX, 21 CFR §888.3080) designed to promote arthrodesis or fusion at a given spinal motion segment. It is typically part of a battery of tests required to demonstrate that a study device is substantially equivalent to a legally marketed predicate device in a 510(k) premarket submission. Alfonso's particle-based model of ASTM F2267-22 can be used to quickly predict the likelihood that a candidate design will perform sufficiently without needing to produce and test a physical prototype. To validate Alfonso's predictions, we compared the load displacement curves of simulated and physical static axial subsidence tests of different sizes of porous 3D-printed titanium-6 aluminum-4 vanadium extra low interstitials (Ti-6Al-4V ELI) transforaminal lumbar interbody fusion (TLIF) devices.

Materials and methods

Preparation and testing of physical specimens

Three different sizes of commercial, US FDA-cleared bullet banana-shaped, 3D-printed porous Ti-6Al-4V ELI (e.g., ASTM F3001 material specification) TLIF devices underwent physical mechanical F2267-22 static axial subsidence tests (n=5 samples of each device size, dimensions are summarized in Table 1). These device designs were chosen for initial validation because they cover a common range of dimensions with a generic shape that is commonly used clinically and are offered by various manufacturers. Intervertebral body fusion devices made of titanium alloys are conventionally used due to their durability and strength, biocompatibility, corrosion-resistance, and higher osteoconductive potential that leads to optimum fusion rates.[1] Material properties for the Ti-6Al-4V ELI (Grade 23) as summarized from manufacturers' sources are listed in Table 3.[2]–[4]

Table 1. Design specifications of the three different sizes of bullet banana-shaped Ti-6Al-4V ELI TLIF devices

Dimensions	Ti-6Al-4V ELI TLIF device		
	Large (H13 mm)	Medium (H11 mm)	Small (H7 mm)
Height (mm)	13	11	7
Lordosis angle (°)	8	8	0
Length (mm)	32	28	28
Width (mm)	10	10	10
Number of specimens	5	5	5

Physical ASTM F2267-22 static axial subsidence testing was performed by an independent certified testing laboratory using the test setup illustrated in Figure 1. For all device sizes, conformal superior and inferior test blocks of grade 15 solid rigid polyurethane (PU) foam (per ASTM F1839-08(2021)) were manufactured with a pocket depth of 1 mm at the deepest point. Material properties for the PU foam grades tested are listed in Table 3.

After placing each device between the corresponding pair of test blocks, compressive load was applied with a hydraulic test frame at a rate of 0.1 mm/s until a certain displacement (10 mm, 8 mm, and 5 mm for H13, H11, and H7 mm spacer, respectively) was reached or unnatural tilting of the implant was observed.

Table 2. Description of the solid rigid PU foam test block, from the Manufacturer's Datasheet and Reported Material Properties based on ASTM D1621 Compressive Tests

Foam grade	Test block dimensions (mm)	Density (kg/m^3)	Volume Fraction	Manufacturer's REF number (original block)	Compressive (based on ASTM D1621)		Speed of sound **c** (m/s)
					Strength (MPa)	Modulus (MPa)	
15 PCF	For H7 mm spacer: 40 x 40 x H32.5 mm	240	0.20	1522-02	4.9	123	871
	For H11 mm spacer: 40 x 40 x H30.5 mm						
	For H13 mm spacer: 40 x 40 x H29.5 mm						

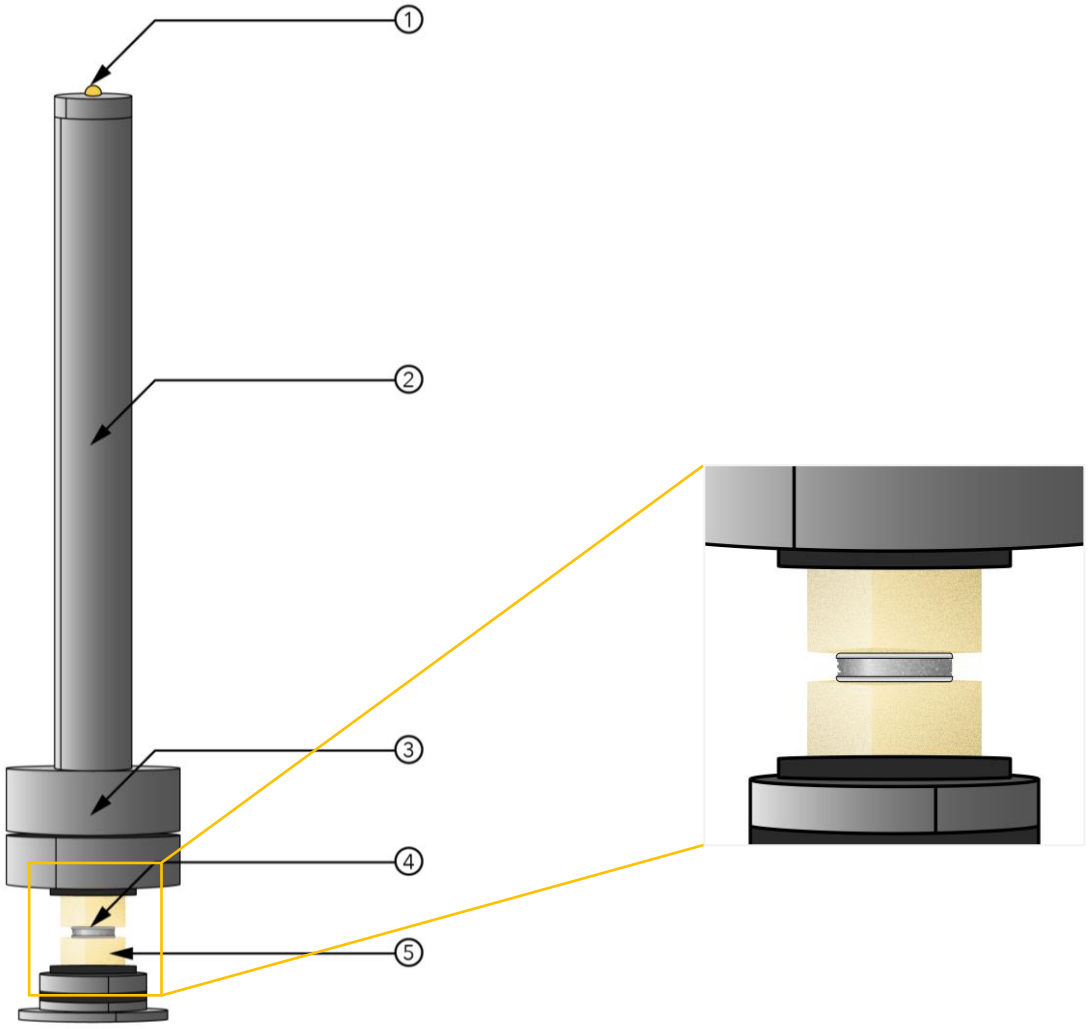

Figure 1. Physical test setup: 1. Ball and socket bearing, 2. Metal pushrod, 3. Spherical bearing, 4. Implant, 5. Foam test block. Illustration by Eka Tjong

Preparation and testing of simulated specimens

Prior to the physical tests, all spinal spacers were scanned by micro-CT at a resolution of 182 µm/pixel (Bruker Skyscan 1076, Bruker Corporation). The DICOM image stacks underwent 3D registration and were converted to particle models of the implant geometry using standard material properties for Ti-6Al-4V ELI as summarized in Table 3 (see "Appendix I: Notes on particle-based methods in *Alfonso*" for further details). Each implant particle model was sandwiched between two simulated grade 15 solid rigid PU foam blocks, with similar dimensions and pocket geometry as the physical testing blocks (see Figure 2). Simulated solid rigid polyurethane foam blocks were prepared by generating particle-based models of 15 PCF foam grades, likewise at a resolution of 182 µm per particle (see "Appendix I: Notes on foam models particle-based methods in *Alfonso*" and [5] for further detail). There were also two outer rigid plates where the force was uniaxially applied to the superior plate for compression with displacement control.

A sensitivity analysis was conducted to determine the maximum uniaxial compression rate (9 m/s), below which there was no observable change in the force–displacement curve. This rate was also much less than the calculated speed of sound of both the PU foam and implant materials (Table 2 and Table 3). Simulated axial subsidence tests were then performed at this rate for all samples. Deviations between the physical and simulated testing protocols and the published ASTM F2267-22 standard are summarized in Table 4. Note that models in *Alfonso*™ do not typically simulate the strain-rate dependent viscoelastic behaviors of materials for static tests; as physical static benchtop tests are usually conducted at very low rates of motion, we consider strain-rate components to be negligible.

The speed of sound c was calculated to set a theoretical upper bound for the rate of motion of the simulation (Table 3):

$$c = \sqrt{\frac{(K_f + \frac{4}{3}G_f)}{\rho}}$$

Where K_f is the bulk modulus, G_f is the shear modulus, and ρ is the density (kg/m^3) of the material.

Table 3. Typical material properties of Ti-6Al-4V ELI from manufacturers' datasheets [2]–[4]

Typical material properties	Ti-6Al-4V ELI (Grade 23)
Density (kg/m^3)	4428.78
Elastic Modulus (GPa)	104.80
Poisson's Ratio	0.342
0.2% Yield Strength (MPa)	827
Ultimate Tensile Strength (MPa)	896
Elongation at break (%)	15
Reduction of Area (%)	45
Speed of sound $\mathbf{c}$ (m/s)	6059

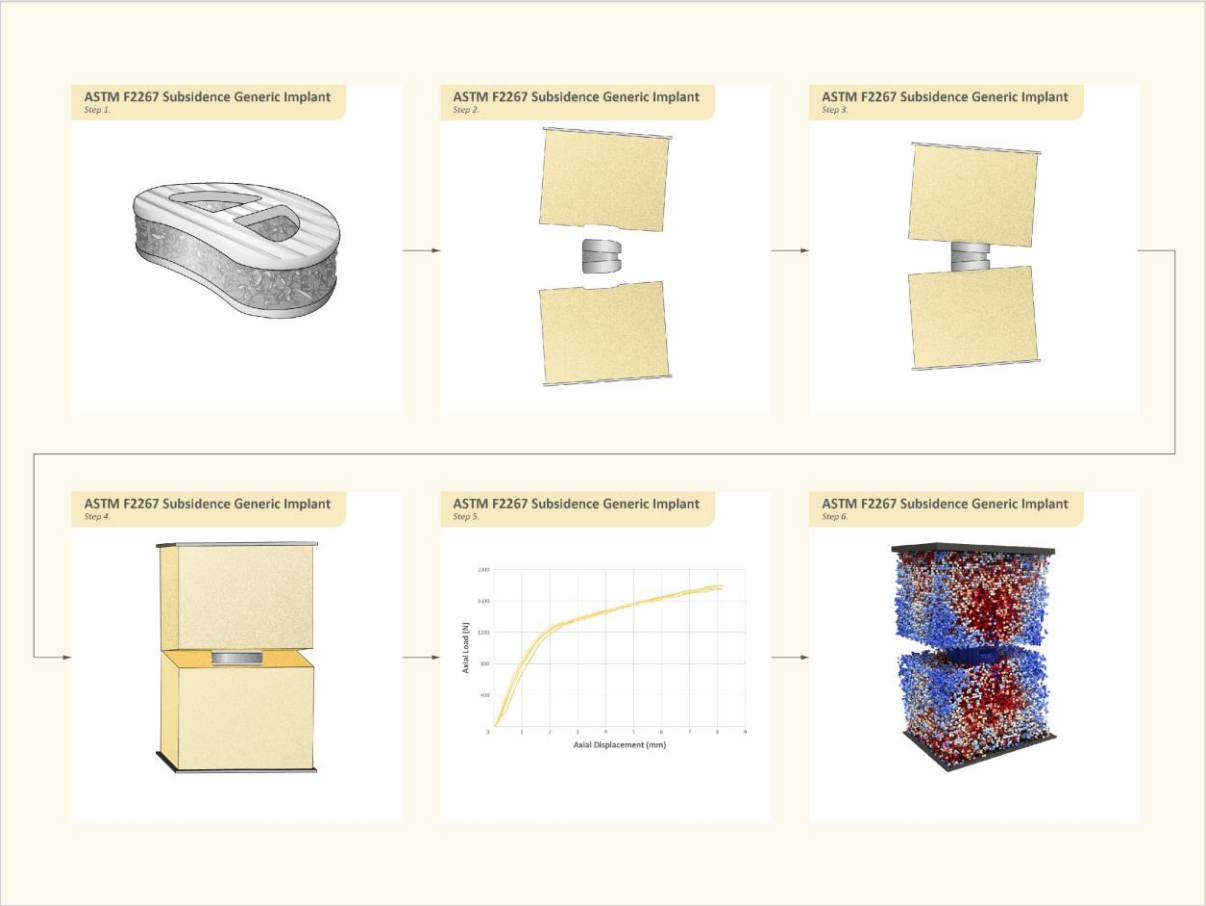

Figure 2. Illustration of the overall ASTM F2267-22 static axial compression test simulation procedure in Alfonso™ Illustration by Eka Tjong

Table 4. Deviations between physical and simulated testing protocols and the published ASTM F2267-22 standard

Test Setup Procedures / Parameters		ASTM F2267-22 Static axial subsidence standard method	Physical test	Simulation
Test setup procedures	Load fixture	(1) Ball and socket joint; (2) Stainless-steel hollow pushrod D25 mm with one 25 mm radius concave spherical end, and other end having ball and socket joint. The length of the pushrod between the center of the ball-and-socket joint to the center of the spherical surface is to be a minimum of 38 cm; (3) The pushrod is connected to the superior fixture by a minimal friction sphere joint (that is, unconstrained in bending and torsion). The inferior spherical fixture is fixed in the base socket.	Follows the ASTM F2267-22 standard, except an inferior spherical fixture was not used to achieve 0 degrees of freedom between the inferior fixture and the test machine base.	Two rigid plates were positioned on the top and bottom of the virtual superior and inferior foam test block, respectively. For the devices with lordosis angle (e.g., 8° angle in H11 mm and H13 mm study devices), the virtual superior and inferior foam test blocks were angled +4° and –4° above and below the horizontal plane, respectively, to mimic the degree of lordosis angle.
	Load application	The actuator of the testing machine is connected to the pushrod by a minimal friction ball-and-socket joint or universal joint (that is, unconstrained in bending). The pushrod is connected to the superior fixture by a minimal friction sphere joint (that is, unconstrained in bending and torsion). The hollow pushrod should be of minimal weight to be considered as a "two-force" member. It thus applies to the intervertebral body fusion device assembly a resultant force directed along the pushrod's axis and located at the center of the superior fixture's sphere joint (the geometric center of the device being tested).	Follows the ASTM F2267-22 standard	The superior rigid plate axially compressed the superior foam block device at a specified rate of displacement. The joints were not modeled in these simulations.

Test Setup Procedures / Parameters		ASTM F2267-22 Static axial subsidence standard method	Physical test	Simulation
	Test block	Two grade 15 PCF solid rigid PU foam blocks as superior and inferior test blocks. The PU foam blocks are to have surfaces that mate geometrically within the intervertebral device similar to how the device is intended to mate with vertebral end plates. Each pair of PU foam blocks shall be used for one test only.	Two grade 15 PCF solid rigid PU foam blocks as superior and inferior test blocks. For each device size, the pocket for each metal block was manufactured using a 0.5 mm milling cutter to match the cage's outer geometry and to have a pocket depth of 1 mm at the deepest point. Each pair of PU foam blocks was used for one test only.	Two virtual 15 PCF solid rigid PU foam blocks as superior and inferior test blocks. For each device size, two virtual PU foam blocks were generated with the pockets matching the cage's outer geometry with a maximum pocket depth of 1 mm. The same virtual PU foam blocks were used across all specimens of the same size.
	Test block height	The linear distance along the Z axis from the top surface of the superior simulated vertebral body to the bottom surface of the inferior simulated vertebral body with the intervertebral body fusion device in position. The block heights shall be 70 mm, 60 mm, and 40 mm for lumbar, thoracic, and cervical intervertebral disc devices, respectively.	70 mm for lumbar intervertebral disc devices	70 mm for lumbar intervertebral disc devices
	Initial intradiscal height	The straight-line distance along the Z axis between the unaltered simulated vertebral bodies. Shall be determined from vertebral body and disc morphometric data at the intended level of application. The user of this test method should select the intradiscal height that is appropriate for the device being tested. The initial intradiscal height shall be constant for all tests for an intervertebral body fusion device assembly of a given size.	11 mm for H13 mm spacer, 9 mm for H11 mm spacer, and 5 mm for H7 mm spacer	Same as the physical test
	Sample size	Minimum of n=5 test samples	n=5 per device	n=5 per device

Test Setup Procedures / Parameters		ASTM F2267-22 Static axial subsidence standard method	Physical test	Simulation
Parameters	Axial compression rate	The load is to be applied to the intervertebral body fusion devices on coordinates (0, 0, *Z*) at a rate of 0.1 mm/s.	0.1 mm/s	9 m/s
	Data collection time interval	Not mentioned; suitable to continuously record load versus load fixture displacement	0.05 s	1×10^{-9} s
	Type of data	Load–displacement data, which will be used to calculate the yield displacement (mm), stiffness (N/mm), yield load (N), ultimate displacement (mm), and ultimate load (N).	Follows the ASTM F2267-22 standard	Follows the ASTM F2267-22 standard
	End point	Not specified, although the load–displacement data should be recorded so that stiffness and yield load can be determined.	Follows the ASTM F2267-22 standard: until a certain displacement was reached (10 mm, 8 mm, and 5 mm for H13, H11, and H7 mm spacer, respectively) or unnatural tilting of the implant was observed.	Up to the maximum displacement of the physical test
	Resolution (specific to simulation)	Not applicable	Not applicable	182 µm

Data and statistical analyses

The load–displacement data were normalized such that zero displacement was set at 100 N for both the physical data and the *Alfonso*™ simulation data, due to adjustment in position and settling of the joint fixtures upon initial loading in the physical test. Stiffness of the system (K_s) in the initial linear-elastic region of physical data and simulation data was calculated in the load range from 200 N to 600 N and 400 N to 800 N, respectively. The stiffness value of the system and the stiffness of the device (K_d) are both necessary inputs for computing the stiffness of the PU foam block (K_p), an indicator of the propensity of an intervertebral body fusion device to subside or migrate into the end plates of the vertebral bodies. The yield load and displacement values were calculated for H11 and H13 mm physical and simulated tests. Yield load value was determined from the load–displacement curve as the applied load required to produce a permanent deformation equal to the offset displacement. Yield displacement was determined from the load–displacement curve as the displacement when an intervertebral body fusion device has a permanent deformation equal to the offset displacement, in which ASTM F2267-22 has specified it to be 2 mm for lumbar implants. Due to the characteristics of the load–displacement curves for H7 mm physical and simulated tests, the yield load and yield displacement were beyond the end point criteria and, thus, they could not be determined.

To provide quantitative comparison of the entirety of the load–displacement graphs, concordance analyses were performed on both physical and simulated datasets. The numbers of data points obtained from the physical tests and *Alfonso*™ simulations varied due to the differences in their data collection sampling rates. We normalized this variance between the data sets using custom Python code designed to perform the necessary interpolation without changing the characteristic shape or magnitude of the curves. Statistical analyses were performed using MedCalc® (MedCalc Software Ltd, Ostend, Belgium).

Note: Lin's concordance correlation coefficient (CCC)

Lin's concordance correlation coefficient (CCC) evaluates the degree to which pairs of observations fall on the 45° line through the origin (i.e., the line of equality). [6], [7] The concordance correlation coefficient is calculated as $\rho_c = \rho \times C_b$ ($-1 \leq \rho_c \leq 1$) where:

- ρ is the Pearson correlation coefficient, which measures how far each observation deviates from the best-fit line, and is a measure of precision, and
- C_b is a bias correction factor that measures how far the best-fit line deviates from the 45° line through the origin and is a measure of accuracy ($0 < C_b \leq 1$; $C_b = 1$ when there is no deviation from the 45° line).

A CCC value of 1 indicates strong concordance, while a value of -1 indicates strong discordance. Borrowing from the standard interpretation of Pearson's correlation coefficient or intraclass correlation coefficients, we assume that positive CCC values <0.20 indicate "poor" concordance, while values >0.80 indicate "excellent" concordance.

Results

No material failure (i.e., crack formation) were found within any of the spinal spacers in both the physical and simulated test cases. The deformation of both superior and inferior PU foam blocks observed in the simulation is represented by the stress and material failure of a dummy device that underwent static axial compression as shown in Figure 3.

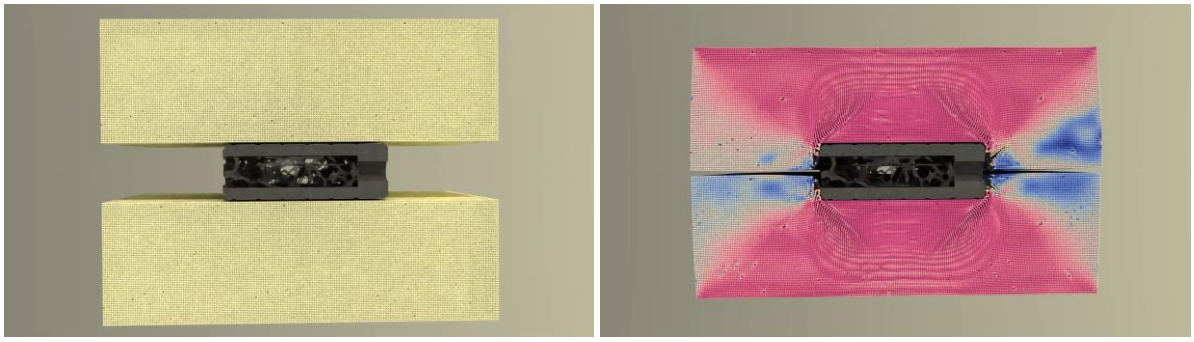

Figure 3. Representative images showing a simulated ASTM F2267-22 static axial subsidence test with a similar dummy device, whereas the actual simulations were conducted using a commercial, US FDA-cleared intervertebral body fusion device.

The average CCC between the load–displacement curves of the physical and simulated tests across all implant sizes was 0.95 (using between 228 and 485 sample points per curve, see Table 5), suggesting excellent concordance.

For the large-sized H13 mm device, the overall physical and simulation load–displacement curves were similar, especially in the yield regions (see Figure 4); the average K_s values were 533 and 420 N/mm in the H13 mm physical and simulated tests, respectively (see Table 5). The average yield load values were 1,690 and 1,821 N at yield displacements of 5.1 and 6.5 mm in the H13 mm physical and simulated tests, respectively. The average CCC between the load–displacement curves of the H13 mm device (see Table 6) in the physical and simulated test pairs was strikingly high with a value of 0.96.

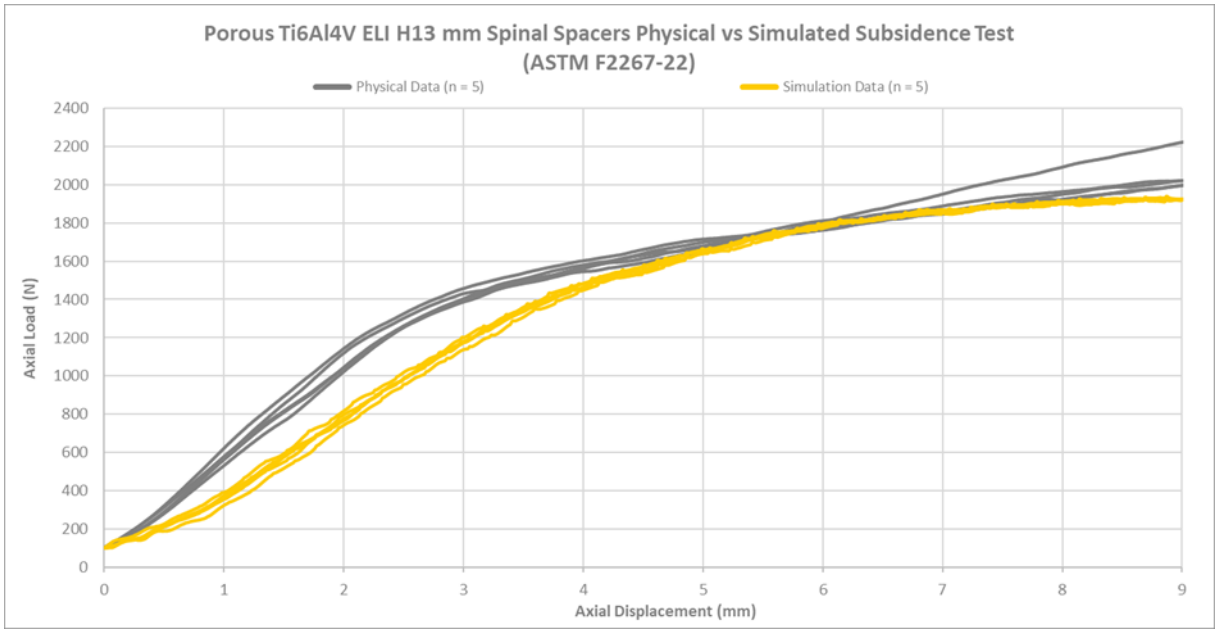

Figure 4. Load–displacement curves from the physical experiment (n = 5) and the simulated (n = 5) static axial compression tests of large-sized H13 mm porous Ti-6Al-4V ELI spinal spacers

For the medium-sized H11 mm device, the overall load–displacement curves were comparable between the physical and simulation data after the yield regions (see Figure 5). The load–displacement curves from the physical data had higher stiffness than those from the simulation data, resulting in the average K_s values of 916 and 443 N/mm in the H11 physical and simulated tests, respectively (see Table 5). The average yield load values were 1,408 and 1,679 N at yield displacements of 3.4 and 5.7 mm in the H11 mm physical and simulated tests, respectively. Fortunately, the overall CCC between the load–displacement curves of the H11 mm device in physical and simulated test pairs was still very high with an average value of 0.91. Note that for the H11 mm device, a different pocket design was created for the simulated virtual PU foam test blocks in comparison to the machined pocket design used in the physical test. The pocket design used in the physical test had more conforming curvature. This may explain the deviation in the load–displacement curves from the physical test versus simulated test for the H11 mm device.

For the small-sized H7 mm device, the overall load–displacement curves were comparable between the physical and simulation data (see Figure 6); the average K_s values were 586 and 457 N/mm in the H7 mm physical and simulated tests, respectively (see Table 5). The yield load and yield displacement for both the physical and simulation data could not be determined from the load–displacement curves given that the offset lines were beyond the end point. The CCC between the load–displacement curves of the H7 mm device in physical and simulated test pairs was very high with an average value of 0.98.

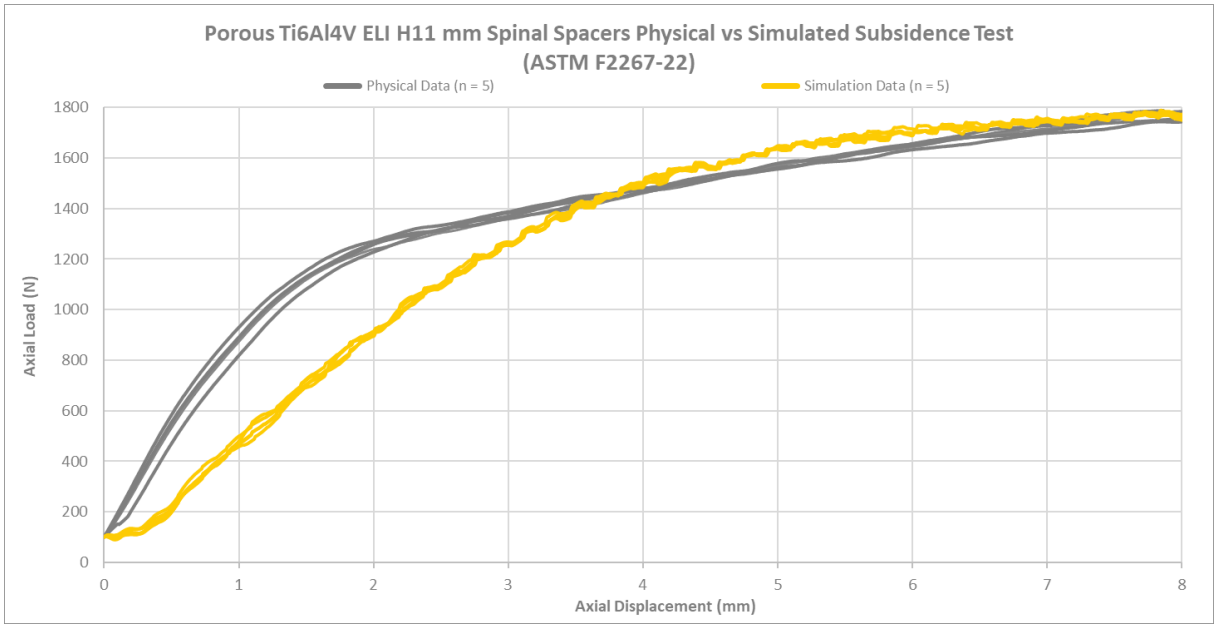

Figure 5. Load-displacement curves from the physical experiment (n = 5) and the simulated (n = 5) static axial compression tests of medium-sized H11 mm porous Ti-6Al-4V ELI spinal spacers

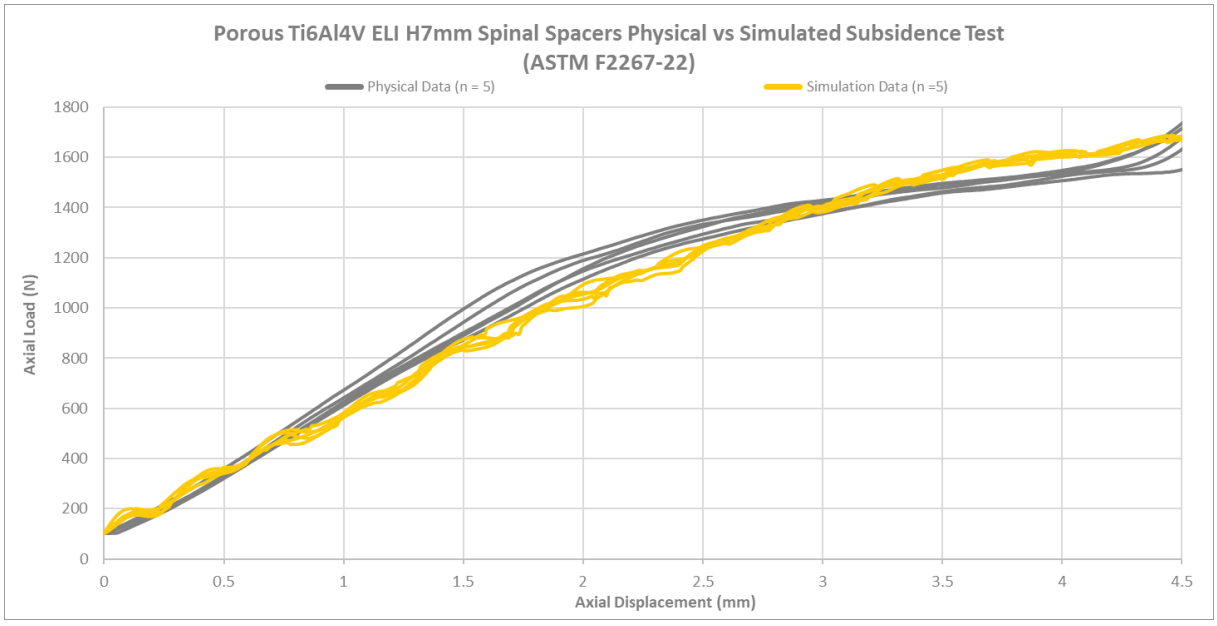

Figure 6. Load-displacement curves from the physical experiment (n = 5) and the simulated (n = 5) static axial compression tests of small-sized H7 mm porous Ti-6Al-4V ELI spinal spacers

Table 5. Calculated values of the stiffness of the system (K_s) from ASTM F2267-22 axial compressive subsidence tests

Specimens	Physical vs Simulation Data for Stiffness of the System (K_s, N/mm)					
	H13 mm, 8°, 32x10mm Spinal Spacer		H11 mm, 8°, 28x10mm Spinal Spacer [1]		H7 mm, 0°, 28x10mm Spinal Spacer [2]	
	Physical	Simulation	Physical	Simulation	Physical	Simulation
Specimen 1	496	426	975	442	603	477
Specimen 2	543	418	897	451	576	422
Specimen 3	571	397	903	448	566	477
Specimen 4	536	435	907	430	578	422
Specimen 5	517	426	900	472	607	487
Average	533	420	916	449	586	457
Standard Deviation	28	14	33	16	18	32
Specimens	Physical vs Simulation Data for Yield Load (N)					
	H13 mm, 8°, 32x10mm Spinal Spacer		H11 mm, 8°, 28x10mm Spinal Spacer [1]		H7 mm, 0°, 28x10mm Spinal Spacer [2]	
	Physical	Simulation	Physical	Simulation	Physical	Simulation
Specimen 1	1,723	1,795	1,414	1,696	n/a	n/a
Specimen 2	1,685	1,827	1,417	1,676	n/a	n/a
Specimen 3	1,696	1,848	1,386	1,682	n/a	n/a
Specimen 4	1,684	1,826	1,405	1,661	n/a	n/a
Specimen 5	1,664	1,810	1,417	1,681	n/a	n/a
Average	1,690	1,823	1,408	1,679	n/a	n/a
Standard Deviation	22	27	13	13	n/a	n/a
Specimens	Physical vs Simulation Data for Yield Displacement (mm)					
	H13 mm, 8°, 32x10mm Spinal Spacer		H11 mm, 8°, 28x10mm Spinal Spacer [1]		H7 mm, 0°, 28x10mm Spinal Spacer [2]	
	Physical	Simulation	Physical	Simulation	Physical	Simulation
Specimen 1	5.4	6.3	3.3	5.8	n/a	n/a
Specimen 2	5.1	6.5	3.5	5.7	n/a	n/a
Specimen 3	4.9	6.7	3.4	5.8	n/a	n/a
Specimen 4	5.1	6.5	3.4	5.7	n/a	n/a
Specimen 5	5.1	6.3	3.6	5.6	n/a	n/a
Average	5.1	6.5	3.4	5.7	n/a	n/a
Standard Deviation	0.2	0.2	0.1	0.1	n/a	n/a

[1] For the H11 mm device, a different pocket design was created for the simulated virtual PU foam test blocks in comparison to the machined pocket design used in the physical test. The pocket design used in the physical test had more conforming curvature.

[2] The yield load and yield displacement for both the physical and simulation data could not be determined from the load-displacement curves given that the offset lines were beyond the end point.

Table 6. Concordance analysis for the ASTM F2267-22 axial compressive subsidence tests

Variables	H13 mm, 8°, 32x10mm Spinal Spacer				
	Physical Data 1 vs Simulation Data 1	Physical Data 2 vs Simulation Data 2	Physical Data 3 vs Simulation Data 3	Physical Data 4 vs Simulation Data 4	Physical Data 5 vs Simulation Data 5
Sample size (curve data points)	435	483	484	483	485
Concordance correlation Coefficient (CCC)	0.9786	0.9602	0.9498	0.9599	0.9487
95% Confidence Interval	0.9748 to 0.9818	0.9539 to 0.9657	0.9420 to 0.9566	0.9536 to 0.9653	0.9403 to 0.9560
Pearson ρ (precision)	0.9914	0.9844	0.9841	0.9867	0.9812
Bias correction factor C_b (accuracy)	0.9870	0.9754	0.9651	0.9728	0.9670
Variables	H11 mm, 8°, 28x10mm Spinal Spacer				
	Physical Data 1 vs Simulation Data 1	Physical Data 2 vs Simulation Data 2	Physical Data 3 vs Simulation Data 3	Physical Data 4 vs Simulation Data 4	Physical Data 5 vs Simulation Data 5
Sample size (curve data points)	404	400	398	397	394
Concordance correlation coefficient (CCC)	0.8892	0.9002	0.9173	0.9008	0.9266
95% Confidence Interval	0.8740 to 0.9026	0.8866 to 0.9121	0.9057 to 0.9275	0.8873 to 0.9128	0.9156 to 0.9362
Pearson ρ (precision)	0.9638	0.9659	0.9710	0.9682	0.9720
Bias correction factor C_b (accuracy)	0.9225	0.9319	0.9447	0.9304	0.9533
Variables	H7 mm, 0°, 28x10mm Spinal Spacer				
	Physical Data 1 vs Simulation Data 1	Physical Data 2 vs Simulation Data 2	Physical Data 3 vs Simulation Data 3	Physical Data 4 vs Simulation Data 4	Physical Data 5 vs Simulation Data 5

Sample size (curve data points)	228	240	230	231	236
Concordance correlation coefficient (CCC)	0.9819	0.9878	0.9892	0.9898	0.9864
95% Confidence Interval	0.9769 to 0.9859	0.9844 to 0.9905	0.9863 to 0.9915	0.9871 to 0.9919	0.9825 to 0.9894
Pearson ρ (precision)	0.9864	0.9896	0.9909	0.9914	0.9883
Bias correction factor C_b (accuracy)	0.9954	0.9982	0.9982	0.9984	0.9981

Conclusion

This validation study suggests that *Alfonso*™ can accurately predict the subsidence behavior of 3D-printed porous Ti-6Al-4V ELI intervertebral body fusion devices of various sizes (e.g., H13, H11, and H7 mm) during axial compression, providing useful supplementary data or replacing physical testing according to ASTM F2267-22 "Standard Test Method for Measuring Load-Induced Subsidence of Intervertebral Body Fusion Device Under Static Axial Compression." The measurement outputs from the *Alfonso*™ simulations of the axial compressive subsidence tests follow the ASTM F2267-22 test standard, namely the load–displacement curve from which we can calculate the stiffness of the system, yield load, and yield displacement. The physical and simulated axial compressive subsidence tests of this study resulted in load–displacement curves with excellent concordance as well as agreement between the slopes of the linear-elastic regions. Beyond the outputs of a physical test, *Alfonso*™ can also provide 3D visualizations of material failure (e.g., plastic deformation, cracking – as stress and strain field data – throughout the entire PU foam and device during subsidence testing. Taken together, this study suggests that *Alfonso*™ can serve as an excellent non-clinical assessment tool in support of pre-regulatory deliberations and regulatory submissions for intervertebral body fusion devices.

References

[1] C. D. Ray, "Threaded titanium cages for lumbar interbody fusions," *Spine (Phila Pa 1976)*, vol. 22, no. 6, pp. 667–669, Mar. 1997.

[2] MatWeb, " Titanium Ti-6Al-4V ELI (Grade 23), Annealed," 2023.

[3] AZO Materials, "Grade 23 Ti 6Al 4V ELI Alloy (UNS R56401)," 2013.

[4] Carpenter Technology, "Ti 6Al-4V ELI," Sep. 2021.

[5] J. Oentaryo, S. Kulper, and E. A. Ueda Boles, "Validation of polyurethane foam models in Alfonso™: Uniaxial compression," 2022.

[6] L. I.-K. Lin, "A Concordance Correlation Coefficient to Evaluate Reproducibility," *Biometrics*, vol. 45, no. 1, p. 255, Mar. 1989, doi: 10.2307/2532051.

[7] MedCalc Software Ltd, "Concordance correlation coefficient." https://www.medcalc.org/manual/concordance.php (accessed May 27, 2022).

Appendix I

Notes on particle-based method simulation in *Alfonso*™

- "Resolution" (e.g., 50, 200, 500 µm) in *Alfonso*™ is typically equivalent to the diameter of the particles in the model, and thereby the minimum distance within which particles begin to interact. The degree of interaction between particles varies continuously as a function of their distance (e.g., in compression, particles repel more vigorously the closer they are to one another, while the reverse is true for tensile forces acting between "bonded" particles of the same object).
- Each particle represents a small volume of mass of an object in the analysis, the material properties of which (elastic modulus, yield, failure, hardening criteria, etc.) dictate the responses of particles to forces applied during analysis.
- Micro-CT scans of the physical intervertebral body fusion devices were collected and reconstructed. For the post-processing steps, the micro-CT scans underwent 3D-registration for alignment ensuring the samples were in similar positions for the simulation setup. The scans were converted to point files upon applying a suitable thresholding value and selection of the region of interest.
- Using the stated material properties from the manufacturer as a starting point, a proprietary scaling factor of the failure mean and standard deviation was applied uniformly to the ultimate strength of Ti-6Al-4V ELI.
- In general, we do not scale material density (i.e., mass) in *Alfonso*™.
- While the initial positions of particles are typically spaced in discrete increments of the resolution (e.g., 182 µm in this particular validation study), during analysis particles may continuously move in 3D space. For instance, a particle initially at (182, 182, 182) may move to (182.0034, 181.793403, 184.09809823462) during analysis.
- "Bonds" between particles in *Alfonso*™ are typically formed only at the initial time state, and then only between neighboring particles of the same object. Bonded particles resist both compression and tension, per the homogeneous or heterogenous properties of the material, until the stress or strain failure limits of the material are exceeded, and a crack is formed. Failed particles remain in analysis (e.g., as debris) and continue to interact with other particles, allowing phenomena such as compaction to be faithfully reproduced in *Alfonso*™.
- "Unbonded" particles that come into contact after analysis has begun (i.e., particles that move to within the minimum distance of interaction) will not form bonds and will only repel one another.
- (See [5] and "Beyond FEA: Particle-based simulation 101" at https://www.lifespans.net/publications for further discussion of the basics of mesh-free analysis)